Quaternary International 514 (2019) 76–84

Contents lists available at ScienceDirect

Quaternary International

journal homepage: www.elsevier.com/locate/quaint

The iBox-FC: A new containment vessel for Itrax X-ray fluorescence core-scanning of freeze cores

Braden R.B. Gregory[a,*], R. Timothy Patterson[a], Eduard G. Reinhardt[b], Jennifer M. Galloway[c]

[a] Department of Earth Sciences, Ottawa-Carleton Geoscience Centre, 1125 Colonel By Dr., K1S 5B6, Ottawa, ON, Canada
[b] School of Geography and Earth Sciences, McMaster University, 1180 Main St. W, L8S 4L8, Hamilton, ON, Canada
[c] Natural Resources Canada/Ressources Naturelles Canada Geological Survey of Canada/Commission Géologique du Canada, 3303 33rd Street N.W., T2L 2A7, Calgary, AB, Canada

ARTICLE INFO

Keywords:
Itrax
Freeze coring
Micro-XRF core scanning
μXRF
Multivariate log-ratio calibration
Log-ratio

ABSTRACT

A combination of Itrax micro-X-ray fluorescence core scanning (μXRF-CS) and freeze coring can facilitate the development of high-resolution (*e.g.* sub-decadal) paleoclimate records in lacustrine systems where low sedimentation rates and poorly consolidated "colloidal soup" at the sediment/water interface prevents retrieval and Itrax-μXRF-CS analysis of undisturbed cores using conventional gravity corers. The iBox-FC containment vessel described and tested here delays thawing of highly perishable freeze cores for up to two hours, providing adequate time to carry out high-resolution Itrax-μXRF-CS analysis. The iBox-FC is comprised of an open-topped Styrofoam box divided into chambers using high-density polyethylene (HDPE) that are filled with freeze pack gel. When the vessel is frozen, core slabs up to 13 cm long may be positioned into a central chamber and then scanned following normal Itrax-μXRF-CS methodology. To test the reliability of μXRF-CS analysis obtained from frozen sediments, a freeze core recovered from Control Lake, Northwest Territories, Canada, was sub-sectioned and analyzed using μXRF-CS and then subsampled for ICP-MS following near-total acid digestion. Comparison of μXRF-CS and ICP-MS results showed strong correlations ($R^2 > 0.8$) for six of nine elements calibrated, and moderate correlations ($R^2 > 0.3$) for the remaining three. Additive log-ratio transformation of data minimized specimen, matrix and edge effects associated with the high porewater contents of the freeze cores and slight melting of the sediment during analysis. These analytical effects had more impact on the lower concentration elements (As, Zn, Ni, Cu) than the higher concentration elements (Ti, K, Mn, Fe, Ca).

1. Introduction

High-resolution paleoclimate and paleoenvironmental reconstructions can be used to study decadal to sub-decadal climate oscillation or discriminate signals of anthropogenic impacts or contamination from the baseline natural variability, which characterizes lacustrine environmental systems (*e.g.* Andrade et al., 2010; Cobelo-Garcia and Prego, 2003; Gammon et al., 2017; Macumber et al., 2018; Roulet et al., 2000). It is difficult to carry out high-resolution paleoclimate or anthropogenic impact studies in lacustrine systems that exhibit low sedimentation rates due to difficulty attaining minimum sample weights required for conventional geochemical analysis. Recent advances in analytical techniques, notably the development of high-resolution micro-X-ray fluorescence core-scanners (μXRF-CS), has drastically reduced the cost, volume of material, and time required for analysis of sediment. Geochemical data can be generated for sediment cores at sub-mm scale through the use of μXRF-CS, and thus permits study of paleoclimate and anthropogenic impacts at a temporal resolution relevant to land use decision makers and planners.

Sediment near the surface-water interface is poorly consolidated in many lacustrine environments. When using conventional gravity coring, material in the upper few centimetres of the core may be homogenized due to its soupy nature if the core is not kept perfectly still during transport and subsequent sub-sampling. Furthermore, this poorly consolidated material may not be cohesive enough for μXRF-CS, creating difficulty when attempting to analyze the environmentally critical uppermost part of gravity cores. Freeze coring freezes sediments *in situ* to the outside of a hollow metal rectangular prism filled with a slurry of dry ice and ethanol (Fig. 1A and B; Shapiro, 1958; Lotter et al., 1997). Freeze coring offers the advantages of preserving the stratigraphy of the sediment-water interface by reducing the risk of homogenization during coring (Fig. 1C). Because of this, freeze coring is ideal

* Corresponding author. 2125 Herzberg Building, Department of Earth Sciences, Carleton University, 1125 Colonel By Drive, K1S 5B6, Ottawa, ON, Canada.
E-mail address: braden.gregory@carleton.ca (B.R.B. Gregory).

https://doi.org/10.1016/j.quaint.2018.09.008
Received 19 December 2017; Received in revised form 30 June 2018; Accepted 11 September 2018
Available online 13 September 2018
1040-6182/

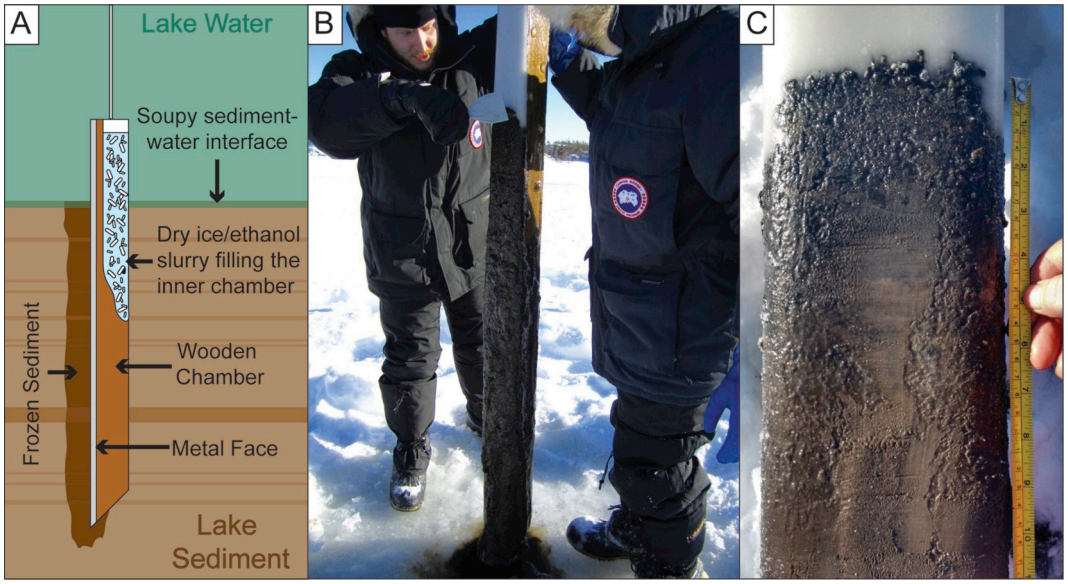

Fig. 1. (A) Cross section of freeze core in sediment. (B) Freeze core recovered from Control Lake, NWT, Canada, and (C) the preserved sediment-water interface of a freeze core retrieved from Control Lake [2 column; online color only]. (For interpretation of the references to color in this figure legend, the reader is referred to the Web version of this article.)

for examining sedimentary records where material near the sediment-water interface is of particular interest.

Combining μXRF-CS with freeze-coring methods could provide high-resolution data within the upper part of sedimentary records, enabling researchers to better examine recent anthropogenic influences on lacustrine systems, study Holocene climate cycles, and bridge the gap between the observed and inferred paleoclimate records (Wittkop et al., 2009; Rydberg et al., 2010; Upiter et al., 2014; Macumber et al., 2018). As of yet, analyzing freeze cores with μXRF-CS has not been attempted due to the logistical difficulties in maintaining freeze core integrity during analysis, which takes place at room temperature for up to 7 h per metre, assuming 0.1 mm resolution and 25 s exposure time per measured interval. This paper describes the construction and application of methods for analyzing freeze cores using the Itrax-μXRF-CS, and provides an example of the analysis and successful calibration of freeze core data using a freeze core recovered from Control Lake, the Northwest Territories (NT), Canada.

2. Construction of the ice-box

In order to maintain the integrity of freeze core slabs during Itrax-μXRF-CS scanning, the sediment must remain frozen. To this end, a small ice Box Freeze Core Holder, henceforth the iBox-FC, was designed to keep cores cold for the duration of analysis (Fig. 2). The iBox-FC consists of an open-topped Styrofoam box separated into chambers by high-density polyethylene (HDPE) sheets that are filled with freeze pack gel (*e.g.* hydroxyethyl cellulose (Cellusize), sodium polyacrylate, or vinyl-coated silica gel). Freeze core slabs placed within the central chamber of the iBox-FC show minimal melting (~1 mm of surface melted) after two hours at room temperature, enough time to scan a 12.5 cm core at 1 mm resolution using a 25 s exposure time per measured interval. Detailed dimensions and instructions for construction of the iBox-FC follow.

Water can cause significant damage to the Itrax core scanner so it is integral to ensure the iBox-FC is constructed water tight. The open-topped insulating box is made using 1.3 cm (1/2") thick Styrofoam wall insulation. Two longitudinal Styrofoam walls 23 cm long by 3.7 cm high, and two lateral Styrofoam walls 8.4 cm long by 3.7 cm high are affixed to a Styrofoam base 11 cm wide, 23 cm long, and 1.3 cm thick using polyurethane glue (Fig. 2A and B). These vessel dimensions place the core surface at an ideal height for the Itrax μXRF detector when the box is placed on the tracks of an Itrax-μXRF-CS at the lowest setting (Fig. 2C). To ensure no liquid leaks out of the box, the joints of the insulating box are sealed with silicon, and a cling film lining adhered to

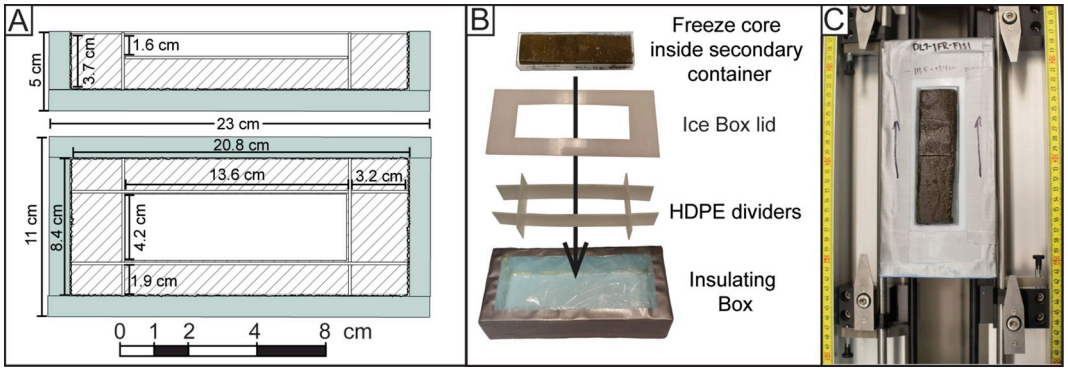

Fig. 2. (A) Cross section (top) and aerial view (bottom) of iBox-FC. Blue fill represents Styrofoam insulation, hatched areas indicate areas filled with freeze pack gel. (B) Exploded view of different pieces of the iBox-FC including the insulating box, the HDPE sheets used to divide the insulating box into 9 chambers, the lid enclosing the freeze pack gel, and the polystyrene box holding a freeze core slab. (C) A fully assembled iBox-FC loaded into the Itrax-μXRF-CS and ready for analysis [2 column; online color only]. (For interpretation of the references to color in this figure legend, the reader is referred to the Web version of this article.)

the inside of the box, again using silicon. Once the glue holding together the insulating box dries, the outside of the box is wrapped in duct tape to further minimize the risk of leaks.

Once assembled, the insulating box is divided into chambers using thin HDPE sheets that will be filled subsequently with freeze-pack gel (Fig. 2). Although HDPE is not a good conductor of heat, use of other materials may cause contamination (*e.g.* metal), or are difficult to work with and more expensive (*e.g.* glass, other plastics). To increase the transfer of cold directly to the core, thin HDPE are used. Two-mm-thick HDPE is a good compromise between facilitating heat transfer and remaining robust enough to maintain its shape when the freeze pack gel expands. Four rectangles of HDPE, two longitudinal rectangles 20.4 cm long by 3.5 cm high and two latitudinal rectangles 8.4 cm wide by 3.5 cm high that are connected using halved cross lap slot joints, divide the inner chamber of the insulating box into 9 chambers as illustrated in Fig. 2B. Once pieced together this frame is placed in the insulating box, which is now divided into nine separate chambers. The outer chambers are then filled with freeze pack gel. The gel should reach as close as possible to level with the top of the internal chambers without going over. The central chamber should be half filled with enough freeze pack gel to ensure that the core slab surface will be level, or just emerging above the outer chambers of the insulating box.

An HDPE lid covers all chambers except the central opening to minimize possibility of freeze pack gel falling out of the iBox-FC. The lid is shaped like a hollow rectangle 20.4 cm long by 8.4 cm wide with the cut out centre of the lid being 13.7 cm long by 4.4 cm wide (Fig. 2B). The central cut-out from the HDPE is used in the central chamber to separate freeze core material from the freeze pack gel.

It is recommended that the freeze core subsample to be scanned be placed in a separate container sized to fit within the central chamber of the iBox-FC (Fig. 2B). This facilitates easy removal of freeze core material from the iBox-FC after scanning, and protects the subsample from possible contamination from the freeze pack gel or the HDPE walls of the inner chamber. The dimensions of the iBox-FC were designed to fit polypropylene boxes purchased from US Plastics Corp. (20 dram flextop box, product #201214) with outer dimensions of 13.4 cm long, 4.1 cm wide and 1.8 cm tall.

3. Preparation of freeze cores

In March 2016, a 103 cm long freeze core (CON01-1FRF1) was recovered from Control Lake, NT, Canada (64.07771° N, −111.13493° W; Fig. 3). Control Lake is a 5 m deep lake with roughly oval shape located ~220 km NW of Yellowknife and just north of the latitudinal treeline in subarctic Canada. Control Lake served as a control site for an environmental study carried out to evaluate the environmental impact of seepage from tailings from the nearby historical Tundra-Salmita gold mine. Control Lake is hydrologically isolated from the flow path that travels from the tailings pond through several small lakes and ponds before connecting to the larger Courageous Lake to the north. In April 2017, CON01-1FRF1 was subsectioned into nine freeze core slabs and transported to McMaster University, Hamilton, ON, Canada, for analysis using Itrax-μXRF-CS.

Freeze cores collected were up to 13 cm wide with a maximum length of 2 m. To obtain subsample slabs sized for use with the iBox-FC, freeze cores were longitudinally and latitudinally sub-sectioned using a hacksaw and a ripsaw. Hacksaws were used for making latitudinal cuts as they minimize loss of material and ripsaws were used for longitudinal cuts as quickly slices through the frozen mud. For the iBox-FC vessel described here, core slabs were cut to ~12.5 cm long and ~3.6 cm wide, which is slightly smaller than the internal dimensions of the inset box. Care should be taken during sectioning to avoid cracking the sediment to minimize analytical problems that may result in invalid data (Fig. 4). The iBox-FC should be completely frozen before core placement to avoid melting. Ceramic knives may be used to avoid contamination if the purpose of the research is trace element analysis.

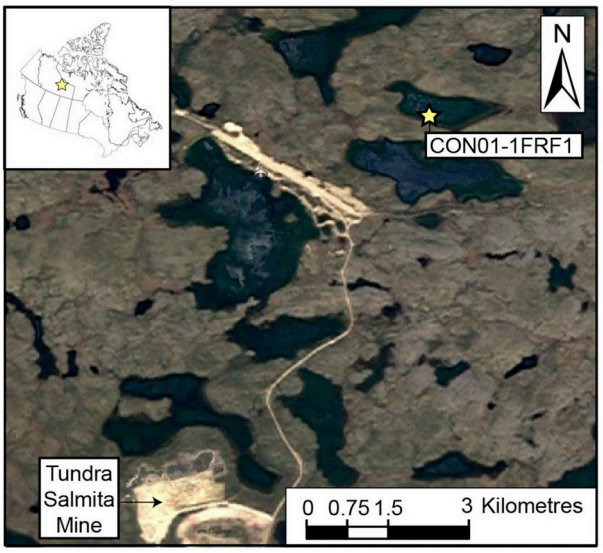

Fig. 3. Map showing the location of CON01-1FRF1 in Control Lake and nearby Tundra Salmita Mine; Inset shows location of Control Lake in NWT, Canada [1 column; online color only]. (For interpretation of the references to color in this figure legend, the reader is referred to the Web version of this article.)

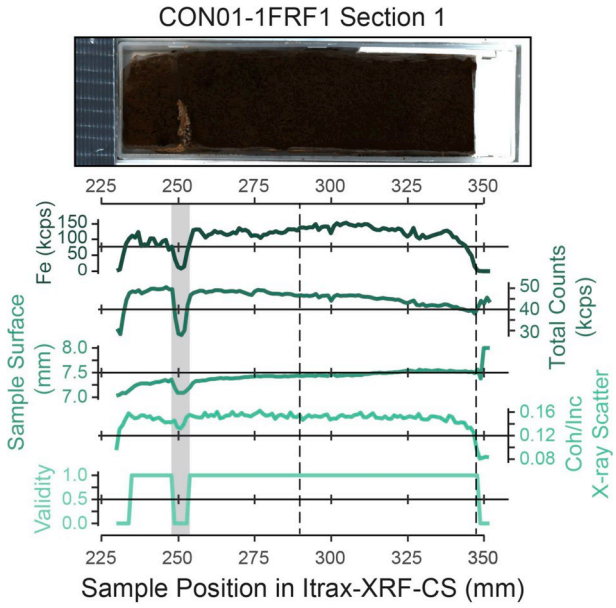

Fig. 4. Comparison of CON01-1FRF1 Section 1 core image to various parameters of practical use to determine start and end point of a core section. The light grey area denotes a cracked portion of the core that resulted in unusable data. The dashed black lines indicate the core depths shown in Fig. 5. [1 column; online color only]. (For interpretation of the references to color in this figure legend, the reader is referred to the Web version of this article.)

Between cuts, slicing implements need to be thoroughly cleaned to minimize possible contamination issues.

For Itrax-μXRF-CS analysis, core slab surfaces need to be made as level as possible to minimize issues caused by surface roughness or analysis of uneven surfaces. HDPE shims were used to level the core slabs prior to analysis, but should be avoided if possible as they reduce the contact of the freeze core slab with the underlying freeze-pack gel. A cleaned glass microscope slide can be used to scrape the surface of the core smooth. A cleaned glass microscope slide was used to scrape the surface laterally across the face of the slab to smooth the surface for analysis.

4. Recommended procedures during analysis

In preparation for analysis, an iBox-FC with contained freeze core slab was removed from the freezer and a 4 μm Ultralene® plastic film (SPEX Centriprep) was affixed to the surface to retain sediment moisture during scanning. To ensure that the film adhered to the core, the surface of the freeze core slab was slightly melted by leaving the freeze core slab at room temperature for roughly half an hour, but a heat gun may also be used. Initial tests were conducted in the summer months at the McMaster University facility, but high air humidity caused droplets of water to form on the Ultralene® plastic film. When freeze cores were reanalyzed during the subsequent winter in low-humidity conditions, little condensation was observed on the core surface. As condensation on the surface of the Ultralene can impact the quality of results, it is recommended that freeze core analysis with Itrax-μXRF-CS be conducted under low humidity conditions; analyses presented here were analyzed during periods of low humidity during November 2016.

Depending on the thickness of the freeze core slab and the ambient temperature, freeze core slabs remained cohesive for at least 2 h. We did not conduct radiographic imaging due to time constraints relating to melting of the core slab. For a 12.5 cm core, it was possible to scan a core segment at 1 mm resolution for 25 s per interval without sediment melting.

CON01-1FRF1 sections one through eight (S1-S8) were analyzed using a Mo-anode at 1 mm resolution, 25 s exposure time, and current and voltage of 22 mA and 25 kV, respectively. Freeze core slabs were analyzed in triplicate, first forward (top-bottom), and then twice in reverse (bottom-top), once at 1 mm resolution and again at 5 mm resolution. The two reverse scans were only conducted on part of the core to provide triplicate analyses. Core slabs were returned to the freezer and allowed to re-freeze between the first scan and the second/third scan. There was no need to return the iBox-FC to the freezer between the second and third scans as the scans collectively took less than 2 h.

In order to maintain optimal μXRF-CS counts between analysis of each core section, either the XRF parameters can be adjusted to maintain constant total counts per second between freeze core sections, or XRF parameters can be kept constant across all core sections. Subtle differences in freeze core slab height relative to the X-ray source between difference iBox-FC runs may influence absolute elemental counts due to X-ray attenuation (Verma, 2007), resulting in shifts in the absolute elemental counts between core sections. It is therefore recommended that XRF parameters be adjusted for each core section to maintain constant counts.

5. Post-analysis data assessment

Analysis of our iBox-FC μXRF-CS results show that minor edge effects regularly occur through the lowermost ~5 mm of slabs analyzed (Fig. 5). These irregularities take the form of an increase in incoherent X-ray scatter peaks, which is concurrent with a decrease in total counts per second (kcps) and concentration of abundant elements (Fe in Control Lake core; Fig. 5B). Although the decrease in incoherent and coherent scatter may represent an increase in lighter elements (Boyle et al., 2015; Duvauchelle et al., 1999), there was no visible change in sedimentology in our testing to suggest that the results may have been caused by an increase in organic matter or water content in the core slab. The higher X-ray scatter peaks may have been due to an increase in the thickness of a layer of water between the core surface and Ultralene film that formed as the core surface slowly melted. If this was the cause, it is expected that there would have been a gradual increase in X-ray scatter during scanning, which was not observed (Fig. 5A and B). Furthermore, the effect was also observed across multiple cores of varying length, suggesting that this phenomenon was not due to the melting of core material (Fig. 5A). An increase in the distance between core surface and detector, possibly due to formation of a fine layer of condensation, is another possible explanation for a decrease in observed kcps. This option was rejected as examination of the Ar record showed no apparent increase coeval with abrupt increase in X-ray scatter (Fig. 5B). It is possible that a change in sample geometry through the lowermost few mm of the core slab caused by preferential melting of the edges of the core during slicing, cleaning, and handling influenced the detected μXRF-CS signal. The Itrax-uXRF-CS is configured under the assumption that samples are positioned at 90° to the X-ray source and the XRF detector 45° to the sample surface (Fig. 6A and B). The trailing edge of the freeze core slabs, due to melting during handling, has a slight curvature that changes the assumed sample geometry (Fig. 6C). Shifts in the angle at which incident X-rays strike a sample surface alters the intensity of detected X-radiation (Bonizzoni et al., 2014; Geil and Thorne, 2014). This change in intensity would cause a shift in the relative concentrations of elements, biasing estimates of relative elemental change in sediment core samples near the edge of the core.

To test if changes in sample geometry influenced XRF measurements, freeze cores were scanned (top-down), then rotated 180° and scanned a second time (bottom-up). Incoherent and coherent X-ray scatter in the bottom-up analysis showed an inverse trend to that observed when freeze core slabs were scanned top-down: a sharp decrease in incoherent and coherent X-ray scatter (Fig. 5C). The inverse trend was also observed in Fe concentrations, with a continual increasing trend observed in the bottom-up reverse-scanned core coeval with a sharp decrease in the top-down-scanned core segment (Fig. 5C). There was no apparent influence of edge effects in elemental log-ratios, indicating that transformation using elemental log-ratios minimizes the observed edge effects.

6. Application of the equipment

Results from Itrax-μXRF-CS were imported into the ItraXelerate software following the recommendations of Weltje et al. (2015). Following the Itrax-μXRF-CS analysis, the freeze core slabs were re-cleaned, and twenty-nine 1 cm long sub-samples were selected for ICP-MS analysis using the results from ItraXelerate calibration analysis as a guideline. Six samples were analyzed in triplicate to provide a measure of absolute geochemical error. Due to the limited material remaining from the freeze core slab, three 1-cm subsamples were combined, allowed to melt, and then homogenized for triplicate analysis of samples. Freeze core subsamples were then submitted to Acme Bureau Veritas, Vancouver, BC, Canada, for ICP-MS analysis. A near total, four-acid digestion was used prior to analysis. Values less than the detection limit in the ICP-MS dataset were converted to 0 values. The standard deviation for elements in the ICP-MS dataset was calculated using the following equation (after McCurdy and Garrett, 2016)

$$\sigma = \sqrt{\left(\frac{\sum_{i=1}^{3}(x_{ijn} - \mu_{jn})^2}{3N}\right)}$$

where x represents replicate measurement i of element j in triplicate set n, μ represents the mean concentration of element j in a replicate set n, and N equals the total number of triplicate sets measured. Because data cannot be loaded into ItraXelerate without SiO values, and because MA-ICP-MS cannot detect silicon, a value of 1 ppm Si was added in order to load the ICP-MS dataset.

To test the influence of edge effects on the ability of Itrax-μXRF-CS to recreate actual geochemical values, two Itrax-μXRF-CS datasets were prepared for calibration. The first, or “original”, dataset represented the entirety of data collect from analysis of freeze core slabs. For the second, or “trimmed”, dataset, analysis results for the lowermost 5 mm from all core scans was removed to eliminate any influence from edge effects. Both datasets were calibrated using the multivariate log-ratio calibration (MLC) method using ItraXelerate software (Weltje et al., 2015). The default sample tolerance in the ItraXelerate software was set to 10 mm. As the triplicate ICP-MS values were comprised of 3 cm of

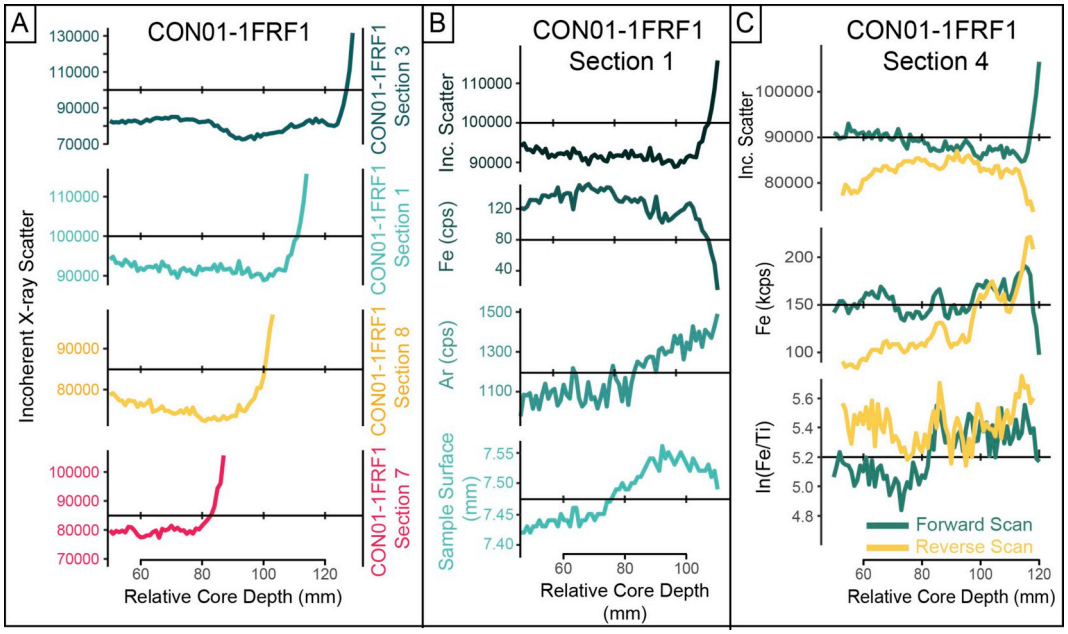

Fig. 5. (A) The final 60 mm of several core sections from CON01-1FRF1 showing an abrupt increase in incoherent x-ray scatter in the lower 5 mm of μXRF-CS core scanning. (B) Comparison of the influence of edge effects as indicated by incoherent scatter to shifts in Fe concentration, Ar concentration, and the surface of the freeze core sample for the last 60 mm of CON01-1FRF1 Section 1. (C) Comparison of Incoherent scatter, Fe (kcps) and ln(Fe/Ti) in the last 60 mm of cores scanned forwards (turquoise line) and in reverse (yellow line) [2 column; online color only]. (For interpretation of the references to color in this figure legend, the reader is referred to the Web version of this article.)

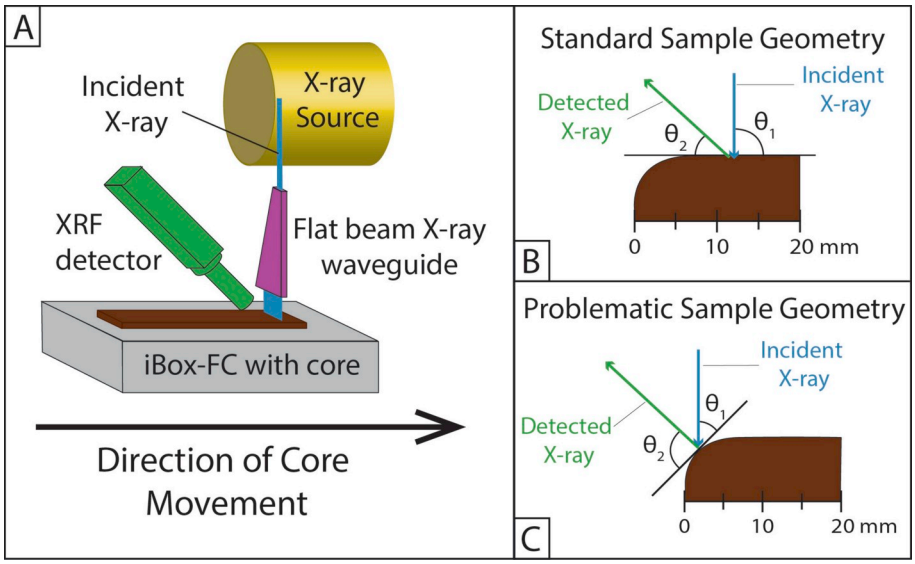

Fig. 6. (A) Schematic diagram of analysis area of Itrax-μXRF-CS showing geometry of X-ray source, incident X-radiation, flat beam X-ray focusing waveguide, XRF detector arranged at 45° to the sample surface, the iBox-FC with freeze core inside it, and the direction of core movement through the analysis area. (B) The standard sample geometry assumed for all Itrax-μXRF-CS analysis showing the incident x-ray (blue), the detected XRF signal (green) and the sample surface (black). θ_1 represents the angle that the incident X-ray strikes the sample surface (90°) and θ_2 the angle of the detector XRF signal relative to the sample surface (45°). (C) Problematic sample geometry hypothesized to be the source of edge effects showing the incident (blue line) and detected X-rays (green line) relative to the sample surface (black line). In this example, the incident x-radiation strikes the sample surface at closer to 45° (θ_1), while the detected X-rays are closer to 90° relative to the sample surface (θ_2). (For interpretation of the references to color in this figure legend, the reader is referred to the Web version of this article.)

sediment, and because the mean sample depth was used to represent depth of geochemical samples, the sample tolerance was increased to 15 mm before calibration was attempted. According to Weltje et al. (2015), the optimal number of elements used for calibration should be roughly one third of the number of unique samples analyzed with conventional geochemistry. Thus, nine elements were selected for calibration: As, Ca, Cu, Fe, K, Mn, Ni, Ti, and Zn. Calcium, Fe, Mn, K, and Ti were selected as they are commonly used as proxies for sedimentation, redox state, or productivity in paleolimnological analysis (Davies et al., 2015), and therefore are likely to be used in lake studies conducted using freeze cores. The remaining four elements (As, Cu, Ni, Zn) were selected as they have a relatively high detection limit for Itrax-μXRF-CS analysis using an Mo-anode, however, these elements were present in lower concentration in our freeze core. The lower concentration of these elements may reduce precision and accuracy of their detection us Itrax-μXRF-CS (Brown, 2015; Cuven et al., 2015; Hunt et al., 2015), but they were included as they are important for our other research in Control Lake. Relationships between observed and predicted values were measured by a goodness-of-fit R^2 value (Table 1). As the calibrated output from ItraXelerate assumed that all calibrated elements sum to unity, and because the nine elements calibrated comprise, on average 8.51% ($\sigma = 2.5\%$, $n = 41$)of the total sample based on ICP-MS results, calibrated results output from the ItraXelerate were converted to proportions of this average percentage.

The edge effects that occur in the last 5 mm of core sections affect all elements included in analysis, not just select abundant elements. Using elemental ratios may thus minimize the influence of these edge effects assuming elements suffer from these edge effects to a similar degree (Fig. 5). Elemental ratios are commonly used μXRF-CS research as they can mitigate specimen and matrix effects for similar reasons. However,

Table 1
Comparison of R^2 predicted Itrax-μXRF-CS results using a multivariate log-ratio calibration to ICP-MS results using the original dataset and a dataset with values influenced by edge effects removed (trimmed dataset). Also shown are the detection limits taken from Qspec software developed by Cox Analytical Solutions and mean elemental concentrations derived from ICP-MS results. [1 column].

Element	Goodness-of-fit R^2		Detection Limit (ppm)	Mean Elemental Concentration
	Trimmed dataset	Original dataset		
As	0.36	0.41	5	75 ppm
Ca	0.95	0.95	23	0.72%
Cu	0.82	0.81	6	66 ppm
Fe	0.95	0.95	7	6.6%
K	0.95	0.94	36	1.0%
Mn	0.9	0.91	8	220 ppm
Ni	0.52	0.53	6	47 ppm
Ti	0.95	0.94	13	0.11%
Zn	0.51	0.53	6	91 ppm

elemental ratios are asymmetrical; conclusions made based on a given elemental ratio (*e.g.* x_1/x_2) cannot necessarily be equated to the inverted ratio (*e.g.* x_2/x_1). This issue can be solved through the use of log-ratios (Aitchison, 1982). We therefore used an additive log-ratio (alr) to transform data using the following equation after Aitchison, 1986 and van den Boogaart and Tolosana-Delgado, 2013:

$$alr(x_i) = \ln\left(\frac{x_i}{x_D}\right)$$

where x_i represents a given element within the calibrated dataset, and x_D represents the denominator element selected from said dataset to which every other element is ratio-ed. For our data, we selected Ti as it is not sensitive to redox changes, was well detected in our analysis, and is commonly used in lacustrine studies using μXRF-CS (Davies et al., 2015).

6.1. Comparison of the original and trimmed datasets

For both the original and trimmed datasets, R^2 values showed strong relationships between observed and predicted results ($R^2 > 0.81$) for six of the nine elements calibrated (Ca, Cu, Fe, K, Mn, Ti; Table 1). Arsenic, Ni and Zn exhibit relatively low R^2 values (< 0.52) in both original and trimmed datasets. The R^2 values for both original and untrimmed dataset were within 0.1 point of each other, with the exception of As that increases from $R^2 = 0.36$ to $R^2 = 0.41$ from the original to the trimmed dataset, respectively. This similarity is expected as removal of the last 5 mm represented a loss of only 4% of the dataset, making both original and trimmed datasets very similar. Comparison of the Itrax-μXRF-CS results with ICP-MS results for both the original and trimmed datasets showed little difference, and the agreement between μXRF-CS and ICP-MS results appeared to increase in both cases through use of alr-transformation (Fig. 7). These results suggest that inclusion of data obtained from intervals of core segments subtly influenced by edge effects does not impact calibration to a large degree, and the alr-transformed dataset can be reliably use for interpretation of μXRF-CS results and calibration.

6.2. Comparison of original dataset to ICP-MS data

The Itrax-μXRF-CS results show strong correlations ($R^2 > 0.81$) for Ca, Cu, Fe, K, Mn, and Ti (Table 1, Fig. 8). These strong correlations are likely due to the high concentration of these elements in sediment, and their high detectability with Itrax-μXRF-CS (Table 1). The strong correlation between μXRF-CS and ICP-MS results indicates that μXRF-CS data provides an accurate representation of geochemical trends in the freeze core for these elements.

Arsenic, Ni, and Zn showed weaker correlations, with R^2 values of 0.36, 0.52 and 0.51 respectively (Table 1, Fig. 8). The poor correlation of As may have been caused by volatilization of As during multi-acid digestion of sediment prior to ICP-MS analysis (Parsons et al., 2012). The combination of geochemical error due to As volatilization in the ICP-MS dataset, and possible attenuation of the μXRF-CS signal associated with high water content and organic matter in the freeze core likely resulted in weaker correlations. Nickel and Zn results, however, are comparable to Cu in terms of atomic size, mass, and detection limits with Itrax-μXRF-CS (< 10 ppm), yet had lower R^2 values than Cu. Both Ni and Zn had relatively low concentrations in the ICP-MS dataset ($\bar{x}_{Ni} = 47$ ppm, $\sigma_{Ni} = 8.7$ ppm; $\bar{x}_{Zn} = 91$ ppm, $\sigma_{Zn} = 13$ ppm; $n = 41$), which may be the cause for weaker correlations as lower concentration elements may show poorer precision in μXRF-CS analysis (Brown, 2015; Cuven et al., 2015; Hunt et al., 2015). However, Cu had a stronger correlation ($R^2 = 0.82$) in spite of similarly low concentration ($\bar{x}_{Cu} = 66$ ppm, $\sigma_{Cu} = 5.2$ ppm, $n = 41$). Sixteen percent of Zn measurements were below detection, possibly explaining the poor correlations, yet, there were no non-detect values in the Ni data, and less than 1% non-detect values for Cu data. Copper concentration determined by ICP-MS has a lower relative standard error (3%) in comparison to Ni (10.5%) and Zn (~6%). Nickel and Zn show weak to moderate positive correlations (Pearson's $r_{Ni} = 0.41$, $r_{Zn} = 0.33$) to the ratio of incoherent/coherent X-ray scatter, whereas Cu shows a weak negative correlation (Pearson's $r_{Cu} = -0.41$). It is possible scatter or absorption effects were influencing μXRF-CS detection of Zn and Ni to a greater degree than Cu. However, as signal attenuation preferentially affects elements with weaker fluorescent energies (Kido et al., 2006), and as fluorescence energies are related to the atomic mass of elements, it is expected that Cu, Zn and Ni should all be affected similarly due to the similarity of their atomic mass. The weak positive correlations observed between X-ray scatter and Ni and Zn may be due to environmental variability rather than signal attenuation as the incoherent/coherent scatter ratio is related to the proportion of water or organic content in core (Boyle et al., 2015; Löwemark et al., 2011). Differences in the analytical procedure may also contribute to poorer correlations since ICP-MS uses a large sample volume (~3 cm^3) in comparison to the volume of sediment analyzed with μXRF-CS that is, depending on the critical depth for a given element and the length of the interval analyzed, generally less than 1 mm^3. The large sample volume provides a better average composition while μXRF-CS maybe detecting subtle sample heterogeneities. This effect would be expected to have a greater negative influence on the lower concentration elements.

Comparison of predicted absolute elemental concentrations from ICP-MS results to μXRF-CS trends showed moderate correspondence for elements with weak or high R^2 values (Fig. 9). The ICP-MS results followed trends similar to that provided by the μXRF-CS data, although in several cases the μXRF-CS data did not fall within two standard deviations of the ICP-MS results. Transforming data using additive log-ratios greatly increased the correspondence between the two geochemical methods. For the alr-transformed data, most ICP-MS results fell within 2 standard deviations of the 10-point running mean of the μXRF-CS data. Considering μXRF-CS and ICP-MS data are compositional in nature, the observed deviations of ICP-MS from non-transformed μXRF-CS data may not be due to issue with calibration, but rather due to closure effects.

To provide a more quantitative measure of the success of elemental normalization in improving the fit of the two datasets, the difference between a 10-point running mean of μXRF-CS and ICP-MS data was calculated, than converted into absolute relative differences based on the mean of μXRF-CS concentrations (Fig. 9, Table 2). For all elements, the mean difference between μXRF-CS and ICP-MS data was greater in the raw μXRF-CS than the alr-transformed μXRF-CS results. Furthermore, raw μXRF-CS tended to have much higher maximum relative differences than did alr-transformed μXRF-CS. This shows that analysis

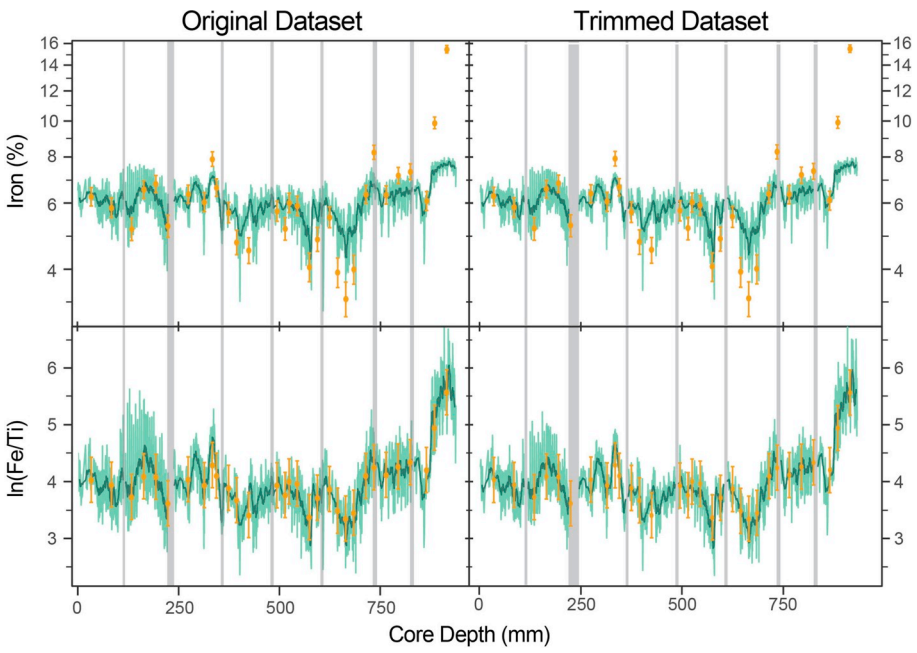

Fig. 7. Comparison of Itrax-μXRF-CS data (light green line) to ICP-MS data (orange circles) for raw Fe and ln(Fe/Ti) for CON01-1FRF1-S1 to S8. Graphs in the left column where created using the original dataset and the graphs in the right column where created using a dataset with all points influenced by edge effects removed. The dark green line represents a 10-point moving average of Itrax-μXRF-CS data. Orange error bars represent two standard deviations of ICP-MS data. The grey bars indicate where data in the original dataset was removed for the trimmed dataset due to edge effects. [2 column; only color only]. (For interpretation of the references to color in this figure legend, the reader is referred to the Web version of this article.)

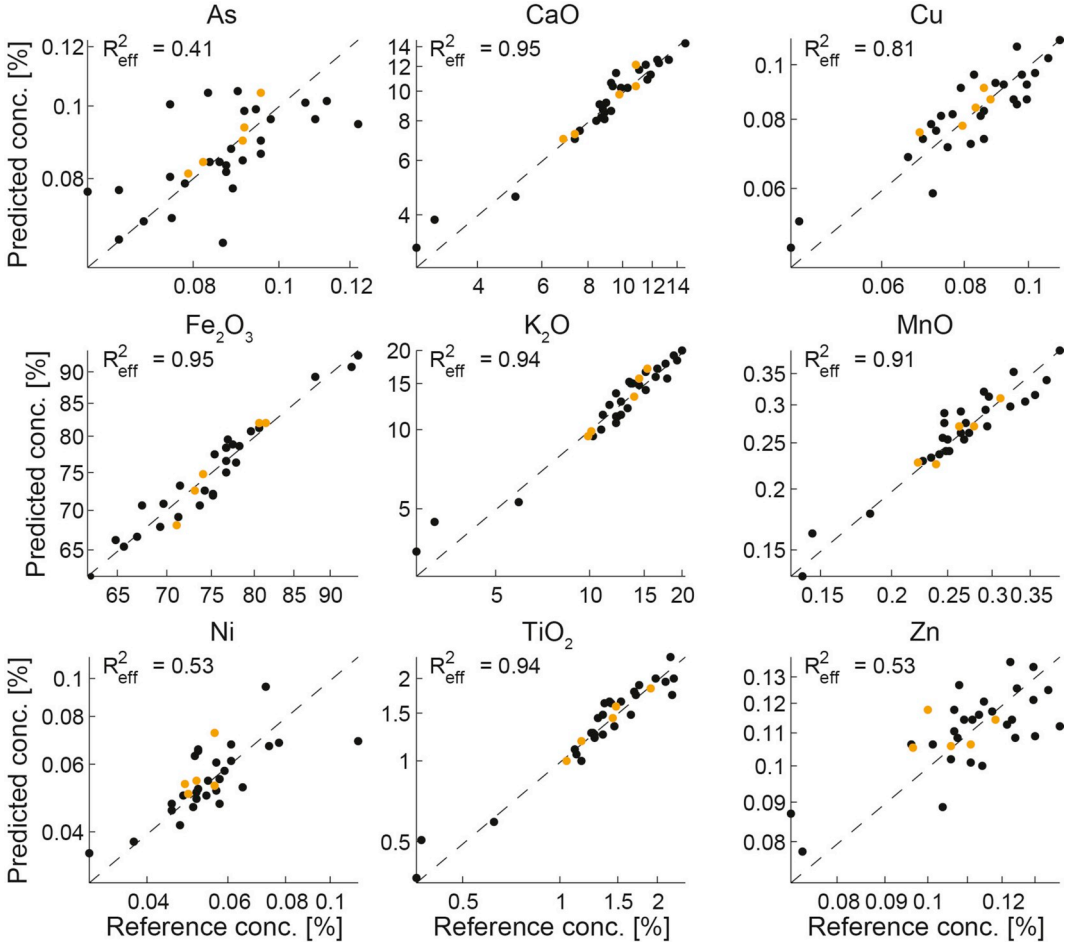

Fig. 8. Output from ItraXelerate multivariate log-ratio calibration of Itrax-μXRF-CS data using ICP-MS data from CON01-1FRF1-S1 to S8. Graphs represent the ability of Itrax-μXRF-CS concentrations predicted using MLC (y-axis) to recreate ICP-MS results (x-axis). Orange dots represent datapoints that may have been influenced by edge effects. [2 column; only color only]. (For interpretation of the references to color in this figure legend, the reader is referred to the Web version of this article.)

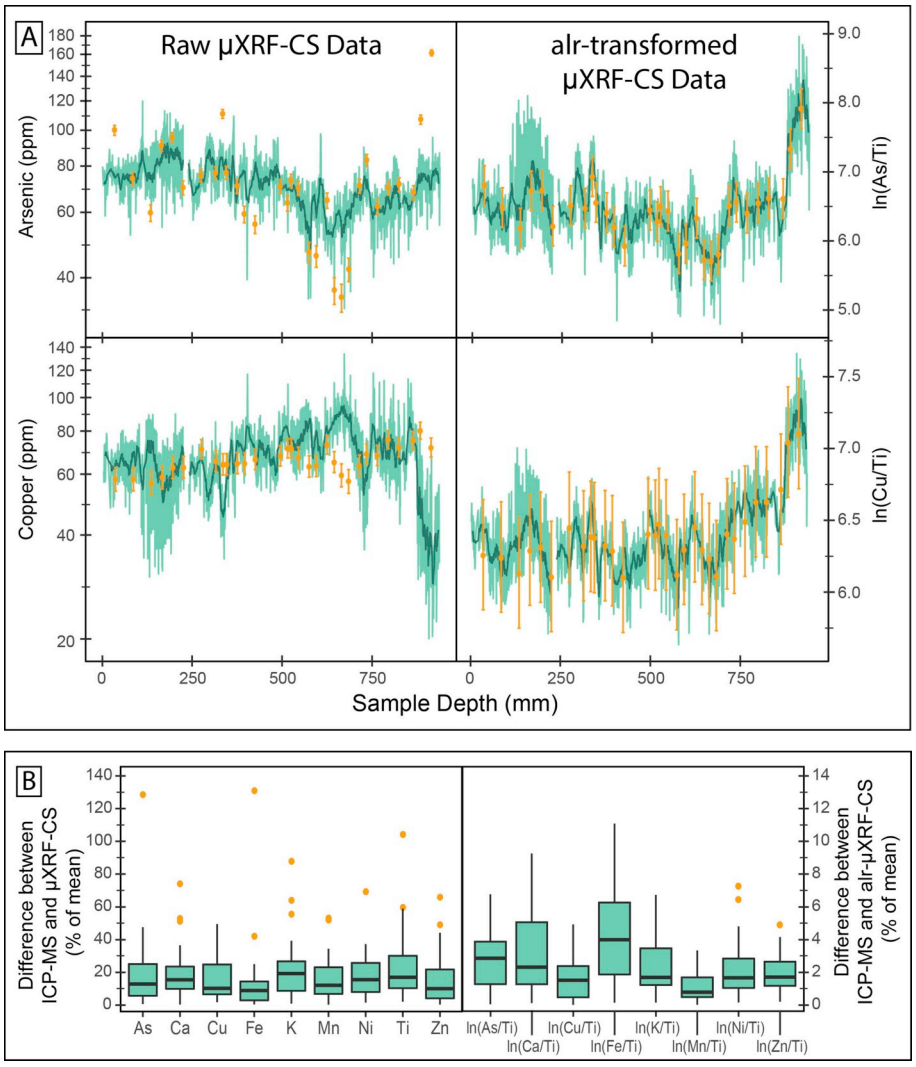

Fig. 9. (A) Comparison of Itrax-µXRF-CS data (light green) to ICP-MS results (orange circles) from CON01-1FRF1-S1 to S8. The dark green line represents a 10-point running mean of Itrax-µXRF-CS results. Orange error bars represent two standard deviations about ICP-MS results. Arsenic and Cu, both elements with lower abundance in Control Lake sediments, but with high detectability with Itrax-µXRF-CS are shown for comparison. The left column shows raw Itrax-µXRF-CS and the right column Itrax-µXRF-CS data that has been normalized to Ti. (B) Boxplots represent the difference between ICP-MS data and the 10-point running mean of Itrax-µXRF-CS in % relative to the mean elemental concentration derived from ICP-MS results. [2 column; online color only]. (For interpretation of the references to color in this figure legend, the reader is referred to the Web version of this article.)

of freeze cores accurately recreated geochemical trends in Control Lake freeze cores and that edge effects can be minimized through use of additive log-ratios, even for elements with poorer correlations.

7. Conclusions

The iBox-FC containment vessel delays thawing of frozen sediments for up to two hours, adequate time to carry out high resolution Itrax-µXRF-CS analysis. Calibration of µXRF-CS values to absolute concentrations based on multi-acid ICP-MS results using the MLC method provides accurate results, with most correlations showing $R^2 > 0.81$. The predicted µXRF-CS trends showed moderate agreement with ICP-MS results when using raw elemental counts; alr-transformation of µXRF-CS data improved the concordance between results obtained using the two geochemical methods. This confirms that µXRF-CS analysis of freeze cores using the above methodology is able to accurately measure geochemical variations in sediment. Transformation of data using elemental log-ratios is therefore recommended before interpretation of results. This transformation minimizes specimen, matrix and edge effects which are prominent issues when analyzing freeze cores which inherently have high porewater content. Even with application of alr-transformation, caution and independent assessment of lower concentration elements is recommended. Despite these limitations, the analytical efficiency of Itrax-µXRF-CS and the high resolution capabilities of the instrument provide significant advantages for the study of recent environmental records in freeze cores, and the iBox-FC

Table 2
Summary statistics displaying the mean, median, 1st and 3rd quartiles (Q1 and Q3) and maximum and minimum differences for the absolute difference between ICP-MS and the 10-point running mean of Itrax-µXRF-CS for all nine elements calibrated using the MLC. Values displayed are in percent relative to the mean concentration of elements based on ICP-MS data. Shown are both raw Itrax-µXRF-CS and alr-transformed µXRF-CS data.

	Fe_{alr}	Fe	Cu_{alr}	Cu	Ni_{alr}	Ni	K_{alr}	K	As_{alr}	As	Ca_{alr}	Ca	Mn_{alr}	Mn	Zn_{alr}	Zn	Ti
Min	0.29	0.25	0.02	1.59	1.01	1.39	0.32	0.80	0.20	0.49	0.23	0.19	0.07	0.13	1.46	0.15	1.90
Q1	5.49	2.79	2.53	6.46	5.50	7.87	2.58	8.59	7.90	5.54	2.55	9.80	3.92	6.71	7.08	4.02	10.1
Median	12.0	8.79	9.33	10.1	8.83	15.4	3.83	19.1	17.0	12.8	4.39	15.4	6.10	12.0	12.3	9.90	16.8
Mean	15.0	14.0	10.1	16.0	13.7	18.2	5.39	22.0	16.6	18.6	5.87	19.0	8.48	16.4	12.2	16.0	24.1
Q3	19.4	14.3	16.3	24.7	16.1	25.6	7.99	26.6	22.4	25.0	8.85	23.4	11.3	23.0	16.8	21.7	30.0
Max	66.2	132	28.0	49.4	60.0	69.9	13.9	88.4	42.7	129	15.5	74.7	25.5	53.8	35.4	66.5	105

allows these capabilities to be used.

Acknowledgements

We gratefully acknowledge funding provided for this project by a Natural Sciences and Engineering Research Council of Canada (NSERC) Engage grant to RTP (Grant #: EGP 482717-15), a Canadian High Arctic Research Station (CHARS)-Polar Knowledge Canada (PKC) grant to RTP and JMG (Grant #: 1516-149), Geological Survey of Canada Environmental Geoscience Program funding to JMG, and a Canada Foundation for Innovation operating grant to EGR, and considerable in-kind support from Seabridge Gold Inc. (transport, lodging). This manuscript represents NRCan contribution number 20180085. We acknowledge Indigenous and Northern Affairs Canada for supporting access to the Tundra-Salmita mine site, and in-kind contributions that included warm meals after long days in the cold Arctic spring.

References

Aitchison, J., 1982. The statistical analysis of compositional data. J. Roy. Stat. Soc. B 44 (2), 139–177.

Aitchison, J., 1986. The Statistical Analysis of Compositional Data. Chapman and Hall, London, pp. 1–416.

Andrade, C.F., Jamieson, H.E., Kyser, T.K., Praharaj, T., Fortin, D., 2010. Applied Geochemistry Biogeochemical redox cycling of arsenic in mine-impacted lake sediments and co-existing pore waters near Giant Mine, Yellowknife Bay, Canada. Appl. Geochem. 25 (2), 199–211. http://doi.org/10.1016/j.apgeochem.2009.11.005.

Van den Boogaart, K.G., Tolosana-Delgado, R., 2013. Analyzing Compositional Data with R. Springer, Berlin.

Bonizzoni, L., Maloni, A., Milazzo, M., 2014. Evaluation of effects of irregular shape on quantitative XRF analysis of metal objects. X Ray Spectrom. 35, 390–399.

Boyle, J.F., Chiverrell, R.C., Schillereff, D., 2015. Approaches to water content correction and calibration for uXRF core scanning: comparing X-ray scattering with simple regression of elemental concentrations. In: In: Croudace, I.W., Rothwell, R.G. (Eds.), Micro-XRF Studies of Sediment Cores: Applications of a Non-destructive Tool for Environmental Sciences, vol. 17. Springer, Germany, pp. 373–392.

Brown, E.T., 2015. Estimation of biogenic silica concentrations using scanning XRF: insights from sutides of Lake Malawi sediments. In: In: Croudace, I.W., Rothwell, R.G. (Eds.), Micro-XRF Studies of Sediment Cores: Applications of a Non-destructive Tool for Environmental Sciences, vol. 17. Springer, Germany, pp. 267–277.

Cobelo-Garcia, A., Prego, R., 2003. Heavy metal sedimentary record in a Galician Ria (NW Spain): background values and recent contamination. Mar. Pollut. Bull. 46, 1253–1262. http://doi.org/10.1016/S0025-326X(03)00168-1.

Cuven, S., Francus, P., Crémer, J.F., Bérubé, F., 2015. Optimization of Itrax core scanner protocols for the micro X-ray fluorescence analysis of finely laminated sediment: a case study of lacustrine varved sediment from the high arctic. In: In: Croudace, I.W., Rothwell, R.G. (Eds.), Micro-XRF Studies of Sediment Cores: Applications of a Non-destructive Tool for Environmental Sciences, vol. 17. Springer, Germany, pp. 279–304.

Davies, S.J., Lamb, H.F., Roberts, S.J., 2015. Micro-XRF core scanning in palaeolimnology: recent developments. In: In: Croudace, I.W., Rothwell, R.G. (Eds.), Micro-XRF Studies of Sediment Cores: Applications of a Non-destructive Tool for Environmental Sciences, vol. 17. Springer, Germany, pp. 189–226.

Duvauchelle, P., Peix, G., Babot, D., 1999. Effective atomic number in the Rayleigh to Compton scattering ratio. Nucl. Instrum. Methods Phys. Res. Sect. B Beam Interact. Mater. Atoms 155 (3), 221–228. http://doi.org/10.1016/S0168-583X(99)00450-4.

Gammon, P., Neville, L.A., Patterson, R.T., Savard, M.M., Swindles, G.T., 2017. A log-normal spectral analysis of inorganic grain size distributions from a Canadian boreal lake core: towards refining depositional process proxy data from high latitude lakes. Sedimentology 64 (3), 609–630. https://doi.org/10.1111/sed.12281.

Geil, E.C., Thorne, R.E., 2014. Correcting for surface topography in X-ray fluorescence imaging. Journal of Synchotron Radiation 21 (6), 1358–1363.

Hunt, E.J., Croudace, I.W., MacLachlan, S.E., 2015. Use of calibrated ITRAX XRF data in determining trubidite geochemistry and provenance in Agadir Basin, Northwest African passive margin. In: In: Croudace, I.W., Rothwell, R.G. (Eds.), Micro-XRF Studies of Sediment Cores: Applications of a Non-destructive Tool for Environmental Sciences, vol. 17. Springer, Germany, pp. 127–146.

Kido, Y., Koshikawa, T., Tada, R., 2006. Rapid and quantitative major element analysis method for wet fine-grained sediments using an XRF microscanner. Mar. Geol. 229, 209–225. http://doi.org/10.1016/j.margeo.2006.03.002.

Lotter, A.F., Renberg, I., Hansson, H., Stöckli, R., Sturm, M., 1997. A remote controlled freeze corer for sampling unconsolidated surface sediments. Aquat. Sci. 59, 295–303.

Löwemark, L., Chen, H.-F., Yang, T.-N., 2011. Normalizing XRF-scanner data: a cautionary note on the interpretation of high-resolution records from organic-rich lakes. J. Asian Earth Sci. 40 (6), 1250–1256. http://doi.org/10.1016/j.jseaes.2010.06.002.

Macumber, A.L., Patterson, R.T., Gammon, P., Galloway, J.M., Falck, H., Swindles, G.T., 2018. Reconstruction of Holocene hydroclimatic variability in subarctic treeline lakes using lake sediment grain-size end-members. Holocene. https://doi.org/10.1177/0959683617752836.

McCurdy, M.W., Garrett, R.G., 2016. Geochemical data quality control for soil, till and Lake and stream sediment samples. Geological Survery of Canada Open File Report 7944, 40.

Parsons, M.B., LeBlanc, K.W.G., Hall, G.E.M., Sangster, A.L., Vaive, J.E., Pelchat, P., 2012. Environmental geochemistry of tailings, sediments and surface waters collected from 14 historical gold mining districts in Nova Scotia. Geological Survey of Canada Open File Report 7105, 365.

Roulet, M., Lucotte, M., Canuel, R., Farella, N., Courcelles, M., Guimaraes, J.-R.D., Mergler, D., Amorim, M., 2000. Increase in mercury contamination recorded in lacustrine sediments following deforestation in the central Amazon. Chem. Geol. 165, 243–266.

Rydberg, J., Klaminder, J., Rosén, P., Bindler, R., 2010. Climate driven release of carbon and mercury from permafrost mires increases mercury loading to sub-arctic lakes. Sci. Total Environ. 408 (20), 4778–4783.

Shapiro, J., 1958. The Core Freezer – a new sampler for lake sediments. Ecology 39 (4) 758-758.

Upiter, L.M., Vermaire, J.C., Patterson, R.T., Crann, C.A., Galloway, J.M., Macumber, A.L., Neville, L.A., Swindles, G.T., Falck, H., Roe, H.M., 2014. Middle to late Holocene chironomid-inferred july temperature for the central Northwest Territories, Canada. J. Paleolimnol. 52, 11–26.

Verma, H., 2007. X-ray fluorescence (XRF) and particle-induced X-ray emision (PIXE). In: Atomic and Nuclear Energy Methods: XRF, Mössbauer, XPS, NAA and B63Ion-beam Spectroscopic Techniques, pp. 1–90.

Weltje, G.J., Bloemsma, M.R., Tjallingii, R., Heslop, D., Röhl, U., Croudace, I.W., 2015. Prediction of geochemical composition from XRF core scanner data: a new multivariate approach including automatic selection of calibration samples and quantification of uncertainties. In: In: Croudace, I.W., Rothwell, R.G. (Eds.), Micro-XRF Studies of Sediment Cores: Applications of a Non-destructive Tool for Environmental Sciences, vol. 17. Springer, Germany, pp. 507–534.

Wittkop, C.A., Teranes, J.L., Dean, W.E., Guilderson, T.P., 2009. A lacustrine carbonate record of Holocene seasonality and climate. Geology 37 (8), 695–698.